Materials Chemistry and Physics 305 (2023) 127974

Contents lists available at ScienceDirect

Materials Chemistry and Physics

journal homepage: www.elsevier.com/locate/matchemphys

Fibrous polypeptide based bioscaffold delivery of minocycline hydrochloride for nerve regeneration

An-Jey A. Su [a], Ning Jiang [b], Shyh-Chyang Luo [b], Kia M. Washington [a], Ming-Chung Wu [c], Yu-Ching Huang [d,*], Wei-Fang Su [b,d,**]

[a] Department of Surgery, Anschutz Medical Campus, University of Colorado, Aurora, CO, USA
[b] Department of Materials Science and Engineering, National Taiwan University, Taipei, Taiwan
[c] Department of Materials Science and Chemical Engineering, Chang Gung University, Taiwan
[d] Department of Materials Engineering, Ming-Chi University of Technology, New Taipei City, Taiwan

HIGHLIGHTS

- A novel drug delivery system was established for neural tissue engineering.
- The release of MH was related to the interfacial behavior between drug and MH.
- Adequate MH concentration enhances biocompatibility.
- Four-fold increase in median neuron length generated on the pristine PBGA scaffold.
- A promising drug delivery system without external stimulations was developed.

ARTICLE INFO

Keywords:
Polypeptides
Glutamic acid
Drug delivery
Minocycline hydrochloride
Scaffold

ABSTRACT

Neural tissue engineering is a technology with the potential to treat irreversible neurodegenerative diseases. We chose poly (γ-benzyl-L-glutamate) (PBG) and its hydrolyzed copolymer (poly (γ-benzyl-glutamate)80-r-(γ–glutamic acid)20) (PBGA) as the raw materials to make fibrous scaffolds by electrospinning process. These raw materials are biocompatible polypeptides which contain the neurotransmitter glutamate. Morphologically, the scaffolds consist of aligned fibers, which is important for directionality. Minocycline hydrochloride (MH) is a neuroprotective antibiotic obviously shown to enhance neurite growth, but is unstable in phosphate buffer solution. By incorporating and immobilizing MH into either PBG or PBGA polypeptide scaffolds, we created a stable drug delivery system. After 7-day release, the cumulative release of MH from PBGA scaffold was 42.65%. Nerve growth factor (NGF) responsive rat pheochromocytoma (PC12) cells were cultured on the scaffold to assess cell biocompatibility and proliferation. We found cell viability and differentiation improved when cultured on scaffolds bearing 2 wt% and 4 wt% of MH. PC12 cells cultured on PBGA incorporating 4 wt% MH exhibited the longest neurite outgrowth of 190.29 μm, the average is 33% increase over that of pristine PBGA after 5-days of NGF mediated differentiation. These polypeptide-based scaffolds loaded with MH are a promising drug delivery system for neural tissue engineering.

1. Introduction

Pathologies of the nervous system are numerous, arising from various etiologies including inherited, chronic neurodegenerative diseases such as Alzheimer's disease, Parkinson's disease, and Huntington's disease. Such disorders are considered, incurable, and largely untreatable diseases of the central nervous system (CNS) due to progressive neuronal cell loss in specific brain regions [1–3]. Recovery from neurodegenerative diseases and acute injuries to the mammalian CNS is complicated by the inability of lesioned axons to regenerate [4]. Outcomes for patients suffering from peripheral nerve injury (PNI) also remain sub-optimal, regardless of surgical intervention, due to distal

* Corresponding author. Department of Materials Engineering, Ming Chi University of Technology, New Taipei, Taiwan.
** Corresponding author. Department of Materials Science and Engineering, National Taiwan University, Taipei,Taiwan.
E-mail addresses: huangyc@mail.mcut.edu.tw (Y.-C. Huang), suwf@ntu.edu.tw (W.-F. Su).

https://doi.org/10.1016/j.matchemphys.2023.127974
Received 17 March 2023; Received in revised form 11 May 2023; Accepted 20 May 2023
Available online 22 May 2023

axonal degeneration following PNI [5]. The use of biomaterials to address the challenges associated with axonal repair in both CNS and peripheral nervous system (PNS) have been actively investigated for decades. Despite the promise of these neural tissue engineering strategies, the need for new highly effective clinical therapies remains unmet [6–8]. Neural tissue engineering combines strategies from cell biology, material science, and engineering to fabricate scaffolds used *in vitro* that mimic the structure and function of natural tissues in order to repair or replace the injured or dead tissue [9,10]. The regenerative capability of artificial scaffolds employed in neural engineered tissue strategies is predicated on biocompatibility, biodegradability, mechanical structure, and extracellular matrix structure mimicry [11,12]. Electrospinning is a versatile technique to spin polymer under high voltage that generates fibrous scaffolds containing micro or nanofibers. Such prepared scaffolds are commonly used in tissue engineering and drug delivery [13,14]. The desired fiber diameter of scaffolds can be adjusted by changing parameters such as applied voltage, polymer solution concentration, solvent ratio, and flow rate of solution. The advantages of fabricating scaffolds by electrospinning technique include easy operation and the adaptability of the process. The simple electrospinning process can produce fibrous scaffolds from lab-scale to industrial-scale with specific orientation, making it practical for medical application [15].

Mechanisms of neuronal cell death are shared across various neurodegenerative diseases, with a cascade of cell death signaling involving oxidative stress, mitochondrial dysfunction and caspase activation, ultimately resulting in apoptosis [16]. Neuroprotective strategies often seek to slow neuron loss associated with neurodegenerative diseases, strokes, traumatic brain injury, spinal cord injury, etc [17]. Minocycline hydrochloride (MH) is a second-generation semi-synthetic tetracycline, with antibiotic properties that inhibit protein synthesis in susceptible organisms [16,18]. Beyond its antibiotic properties, MH has anti-inflammatory and antiapoptotic properties [19]. The neuroprotective effect of MH has been extensively reported in both experimental models and clinical trials [20–23]. Additionally, MH is reported to potentiate nerve growth factor (NGF)-induced PC12 neurite outgrowth, depending on concentration [24]. In experimental models, dosages for MH range from 10 to 50 mg/kg initial dosage (i.v., i. p., v. o.) with supplemental doses at 12–24 h (q12h-24h) [25,26]. Clinically, MH is administered for bacterial infections at 200 mg/day, followed by 100 mg/12h (i.v., v. o., q12h). For acute spinal cord injury, 400 mg is given intravenously (i.v., q12h) with an 800-mg loading dose. In either case, repeated dosing is necessitated by the relatively short half-life of MH *in vivo* (plasma half-life ranges from 11 to 23 h) [27]. Therefore, controlled, and sustained drug-delivery is desirable for administration of MH. Material scientists can fabricate and modify synthetic polymers that leverage mechanical strength properties to customize their application as fibrous scaffolds for tissue engineering. An optimized drug delivery system from fibrous scaffolds should have homogeneous distribution of a drug (or other bioactive molecule) in the fibers, predictable drug release at a determined rate, and drug stability when incorporated in the system over a period of time [28]. Thus, the compatibility between drug and polymer is a critical consideration in designing these systems.

We previously demonstrated poly (γ-benzyl-L-glutamate) (PBG) and poly (γ-benzyl-L-glutamate)-*r*-poly (L-glutamic acid) (PBGA) as biomaterials that can successfully promote neurite outgrowth [29]. In this study, we fabricated PBG and PBGA polypeptide scaffolds containing the neuroprotective drug MH. The release profiles of MH from the scaffolds were systematically studied which is related to the interfacial behaviors between drug and materials. We hypothesized that adding MH to the scaffolds would enhance NGF-induced PC12 neurite outgrowth. We predict that the extent of enhancement would depend on MH concentration in the scaffold. Here, we present results that show a tissue engineering scaffold-drug delivery system based on polypeptide-fibrous scaffolds containing neuroprotective MH for potential application in neural regeneration.

2. Materials and methods

2.1. Chemicals and materials

Chemicals used for the synthesis of PBG, PBGA include L-glutamate acid-benzyl ester (99% purity; Flurochem), triphosgene (98% purity; Sigma), sodium (99% purity; Sigma), dichloroacetic acid (99% purity; Acros), 33 wt% HBr in acetic acid (99% purity; Acros), sodium hydroxide (98% purity; Acros), trifluoroacetic acid (99.5% purity; Acros), tetrahydrofuran (THF, 99% purity; Macron), dimethylformamides (DMF, 99.8% purity; Macron), N,N-dimethylacetamide (DMAc, 99.8% purity; Sigma). Anhydrous solvents of ethyl acetate (EA; 99.5% purity) and benzene (99.7% purity; Sigma) were prepared from the dehydration of the purchased ones by drying with 4A molecular sieves (4–8 mesh; Acros) and N_2 purging overnight. Polycaprolactone (PCL, mol. wt. 282 KDa, PDI:1.3, Sigma) was used as a control polymer in this study. Minocycline hydrochloride (MH, 98.0% purity, cat. #M2288, TCI) was purchased from TCI company.

Reagents used for cell culture including RPMI-1640 culture media (cat. # SH30011.02; Hyclone), nerve growth factor (NGF, cat. #N6009; Sigma), dimethyl sulfoxide (DMSO; cat. # SU01551000; Scharlau), trypsin-EDTA 10x (cat. #03-051-5B; Biological Industries), fetal bovine serum (FBS; cat. # 04-001-1A), horse serum (HS, cat. # 16,050,122; Gibco), antibiotic antimycotic solution 100x (PSA, cat #A5955; Sigma-Aldrich), PBS phosphate buffered saline solution (cat#BP3991, Fisher BioReagents). The solution of trypsin-EDTA 1x was prepared by diluting trypsin-EDTA 10x with PBS.

Chemicals for characterization of *in vitro* assays included Live/Dead viability/cytotoxicity kit (cat. #L3224; Molecular Probes), Alamar Blue cell toxicity assay (cat. #BUF102A; Serotec), bovine serum albumin (BSA; cat. #B4287; Sigma-Aldrich), formaldehyde (37 wt%; cat. # 50-00-0; ACROS Organics) and Triton X-100 (cat. #X198-07; J.T. Baker). The stock solution of phalloidin was prepared by dissolving 0.1 mg phalloidin-TRITC in 1 mL DMSO (76.6 μM). The stock solution of 4',6-diamidino-2-phenylindole (DAPI, cat. #D8417, Sigma-Aldrich) was prepared by dissolving DAPI in DI water (1 mg/mL), phalloidin-tetramethyl rhodamine B isothiocyanate (phalloidin-TRITC, cat. #P1951, Sigma-Aldrich).

Nomenclature

Polycaprolactone is abbreviated as PCL. Two kinds of polypeptides are used in this study: poly (γ-benzyl-L-glutamate) (PBG) and poly (γ-benzyl-L-glutamate)-*r*-poly (α-L-glutamic acid) (PBGA). The monomer of PBG, γ-benzyl-L-glutamate N-carboxyanhydride, is named as BGNCA. The minocycline hydrochloride is named as MH.

2.2. Polymeric material synthesis and characterization

The polymeric materials were synthesized according to the literature [29] and briefly stated below. To synthesize BGNCA monomer, 6 g of L-glutamate acid γ-benzyl ester was added with 180 mL of anhydrous ethyl acetate. 3.75 g of triphosgene was added to the flux. The reaction was proceeded for 2 h at 105 °C under N_2, and the solution was cool down to room temperature for 15–30 min after the reaction was completed.

The NCA solution was poured into hexane, forming white BGNCA precipitate, and was stored at −20 °C for 1 day. The crude NCA was filtered and dissolved in the least amount of anhydrous ethyl acetate, and enough hexane was added into the NCA solution until a little white NCA crystal appeared. The crystallization process was continued at 4 °C overnight. The recrystallize process was repeated 3–4 times until the NCA formed shining white crystals, indicating that the NCA was pure enough to be polymerized. The purified NCA was dried at 40 °C in vacuum oven (Thermo Scientific 3608) for 1 day.

Three grams of BGNCA crystals were placed into the flask and dried

under vacuum for 1 h to remove moisture. 300 mL of benzene was transferred to the flask under N_2. Afterward, sodium methoxide solution was added to the flask all at once with stirring (molar ratio of initiator: monomer = 1:100). The solution became clear and viscous after several minutes. The polymerization was conducted for 48 h and then was precipitated in ether. After precipitation, the polymer was dried in a vacuum oven at 40 °C overnight.

To synthesize PBGA, 1 g of PBG was put in a 50 mL flask and 25 mL of dichloroacetic acid (DCA) was added to the flask. The PBG was dissolved in the solvent overnight. After the polymer was fully dissolved, 760 μl of HBr solution (33 wt% HBr in acetic acid) was added to the flask, reacting for 40 min at 31 °C. Then the reactant was precipitated in ether with a minimal volume of methanol, stirring for 10 min. To purify, the precipitated polymer was re-dissolved in the least amount of THF and precipitated in ether several times. The polymer was dried in vacuum oven in 40 °C, yielding PBGA.

The chemical structures of synthesized PBG and PBGA were characterized by spectroscopies of NMR (Brucker; DPX400) and ATR-FTIR (PerkinElmer; Spectrum 100), respectively. 5–10% (w/v) of polymer was dissolved in trifluoroacetic acid d-solvent for ^{1}HNMR analysis. The polymer films of PBG and PBGA used for IR measuring were made by drop casting of the tetrahydrofuran (THF) solution. The NMR and IR spectra of products are shown in supporting information (Fig. S1, Fig. S2, and Table S1).

The molecular weight of PBG was determined by gel permeation chromatography (GPC) with 0.5% (w/v) polymer solution in dimethylformamide (DMF). The average molecular weight of the PBG was controlled in the range of 200 K–300 K Dalton for the ease of electrospinning process and good quality of the fibers. The results are listed and discussed below in Results and Discussion.

2.3. Scaffold fabrication and characterization

The set-up for electrospinning is shown in the supporting information (Fig. S3). The process typically involved for the polymer solutions of PCL, PBG, and PBGA with 2 wt%, 4 wt%, and 6 wt% of MH was prepared respectively using co-solvent of THF and DMAc overnight. A grounded, rotating collector was placed 15 cm away from the needle tip. For thick fibrous samples (scaffold mat) used in drug release test and mechanical properties test, the collector was first wrapped with aluminum foil and fibers were collected on it for about 20 min; then the mat was covered with wax paper, which made the scaffold mat easier to be removed. For cell test, aluminum foil was wrapped on the collector, and glass coverslips were pasted on the aluminum foil to collect fibers. The preparation of solution and electrospinning parameters were listed in supporting information Table S2. The thickness of mat was controlled in 50–70 μm by the electro spinning time of the fiber fabrication. The thickness was determined by micrometer. The porosity of the mat was controlled in 80–90% by varying the spinning time of fiber fabrication. The porosity was determined by Hg porosimetry.

2.4. Drug release

Thick scaffold mats were removed from the wax paper and cut into 2 × 2 cm^2 pieces. For each test scaffold pieces weighing at least 15 mg are placed in a sample bottle containing 10 mL PBS. For each time point (2, 4, 8, 24, 48, 96, and 128 h), 1 mL PBS supernatant was removed from the sample bottle to measure the released MH, and an equal volume of 1 mL fresh PBS was added to the bottle. The concentration of MH released from the polymer scaffold was measured by UV–Vis spectrometer with a calibration curve made at wavelength 245 nm. Each test was repeated three times. The cumulative release was calculated by the following equation.

$$Cumulative\ release(\%) = \frac{weight\ of\ the\ drug\ released}{weight\ of\ the\ total\ drug} \times 100$$

2.5. Kinetic modeling for drug release

The drug release profiles were fitted with either Higuchi equation or Korsmeyer-Peppas equation [30]. Linear or nonlinear fitting was applied on release profiles using software Origin (Orglab8, OriginLab USA). The cumulative release Q_t at time t is defined as

$$Q_t = \frac{M_t}{M_\infty} \times 100\%$$

where M_t is the cumulative amount of drug release at time t and M_∞ is the total amount of drug release.

The Higuchi equation is

$$Q_t = A\sqrt{D(2C_0 - C_s)C_s t}$$

where D is the diffusion coefficient, C_0 is the initial drug concentration, C_s is the drug solubility in matrix. The equation can be simplified to

$$Q_t = K_H t^{\frac{1}{2}}$$

The Korsmeyer-Peppas equation is

$$Q_t = Kt^n$$

where parameter n characterizes the mechanism of release profile. When $n < 0.45$, the drug release mechanism follows Fick's diffusion; when $0.45 < n < 0.89$, it is non-Fick's diffusion, involving skeleton dissolution [31–33].

2.6. Procedure for in vitro study

Pheochromocytoma 12 (PC12) cell line was used for all the cell tests in this study. The cells were supplied by Dr. T. K. Tang of Institute of Biomedical Sciences, Academia Sinica, Taiwan. Cells were cultured in RPMI-1640 culture media with 10% (v/v) horse serum, 5% (v/v) fetal bovine serum, and 1% (v/v) penicillin/streptomycin/amphotericin B (PSA) at 37 °C under 5% CO_2. The cell seeding density varied for individual experiment and are listed in Table 1. In the case of cell differentiation, the original culture media used to seed cells was removed after 1 day of culturing in RPMI-1640 culture media, and replaced with NGF (100 ng/mL) in RPMI to stimulate the outgrowth of neurites. The culture media with NGF was renewed every 3 days.

2.7. Characterization for biocompatibility of scaffolds

The biocompatibility of materials was characterized by using Live/Dead Assay Kit (Molecular Probes). PC12 cells were seeded in sterile 24 wells cell culture plates of polystyrene (cat. #351147, Falcon). At specific time points (1, 5 days), culture media was removed, and samples were washed with PBS solution (Fisher BioReagents) at room temperature. Then cells were stained with 0.05% (v/v in PBS) calcein-AM for live cells and 0.2% (v/v in PBS) ethidium homodimer-1 for dead cells at room temperature for 45 min. After staining, solutions were removed, and samples were washed with PBS. The samples were restored in 500 μL PBS and were examined by fluorescence optical microscope (CKX41; OLYMPUS) at 100X magnification. For statistically relevant results, each material was repeated 3 times and 5–6 pictures were taken for cell counting. Cell counting was conducted using ImageJ software (U.S. National Institutes of Health, Bethesda, Maryland, USA).

Table 1
Cell seeding density for different experiments.

Experiment	Cell Density (cells/well)
Live/Dead Assay	20,000
Alamar Blue Assay	20,000
Cell Differentiation	5000

2.8. Characterization of cell viability on scaffolds

The scaffold effects on cell viability on was analyzed by Alamar Blue Assay IABA) (ABA solution, cat. #BUF102A; AbD Serotec). PC12 cells were seeded at initial density, then at specific time points (1, 3, 5 days), the culture media was removed, and then replaced with 500 μL of 10% Alamar Blue solution (v/v in DMEM) and put into the 37 °C, 5% CO_2 incubator for 4 h. Three wells with ABA solution without cells served as assay blanks. After incubation, the ABA solution was completely removed and then transferred by pipette to a 96-well plate with 100 μL per well. The remaining adherent cells were washed with PBS and fresh culture media was added prior to placement back into incubator. The reacted ABA solution was analyzed with an absorbance microplate reader (800 TS; BioTEK). The % reduction of Alamar Blue after the cell culture is calculated according to the following equation:

$$\%\ \text{reduction of Alamar Blue} = \{[(O_1\text{-}A_1)\text{-}(O_1\text{-}A_2)]/[(R_1\text{–}N_2)\text{-}(R_2\text{–}N_1)]\} \times 100$$

Here O_1 = molar extinction coefficient (E) of oxidized AlamarBlue at 570 nm = 80586, O_2 = E of oxidized Alamar Blue at 600 nm = 117216, R_1 = E of reduced Alamar Blue at 570 nm = 155677, R_2 = E of reduced Alamar Blue at 600 nm = 14652, A_1 = absorbance of test wells at 570 nm, A_2 = absorbance of test wells at 600 nm, N_1 = absorbance of negative control well (blank) at 570 nm, N_2 = absorbance of negative control well (blank) at 600 nm.

2.9. Characterization for cell differentiation on scaffolds

Cells were stained with DAPI and phalloidin for nucleus and F-actin. Formaldehyde (3.7% v/v in PBS) was added to fix cells for 15 min at room temperature. After fixation, Triton-X 100 solution (1% v/v in PBS) was added to permeabilize cell membranes for 10 min at room temperature. Then, phalloidin solution (1% v/v in PBS) was added to the samples to stain F-actin. After staining for 1 h at room temperature, DAPI solution (0.2% v/v in PBS) was then added to sample wells to stain cell nuclei for 5 min at room temperature. The samples were washed with PBS and restored in PBS for microscopy.

F-actin labeling was used to measure neurite outgrowth. The neurite length was manually measured from the nucleus to the end of the neurite using ImageJ. Each experimental condition was repeated in triplicate, and 77–126 neurites were analyzed.

2.10. Statistical analysis of data

In this study, Kruskal-Wallis one way analysis of variance, H-test was used to determine the significant differences between data groups. When p-value <0.05 means significant difference between groups, indicated by *; p-value <0.01 means there is a high degree of difference between groups (highly significant), represent by **; p-value <0.001 means there is an extremely significant difference between groups (extremely significant), represent by ***. Differences between groups with p-value >0.05 are not statistically significant and are not marked.

3. Results and discuission

Three kinds of 3D scaffolds with aligned fibers were made from PCL, PBG, and PBGA respectively using electrospinning process. For each polymer, four kinds of samples were prepared that were incorporated with either 2 wt%, 4 wt%, 6 wt% MH or without any MH, respectively. PCL is a common biomaterial [34] which was used as a control scaffold. The materials properties and release profile for each scaffold (n = 12) were investigated. PC12 cell viability and proliferation on each of these scaffolds was studied and analyzed. Fig. 1 shows the schematic diagram of this drug delivery system.

3.1. Characterization of polymeric materials for fibrous scaffolds

The polymeric materials, PBG and PBGA, were synthesized according to the reactions shown in Fig. 2. The synthetic yield for PBG was good at 84.2%; we were able to produce partially hydrolyzed PBG (PBGA containing 20 M % of glutamic acid in PBG) with a reasonable yield of 74.4%. GPC was used to characterize the molecular weight of PBG with DMF as a mobile phase. The average molecular weight of PBG was controlled between 200 and 300 kDa for the ease of scaffold processing and good quality fibers. The results are summarized in Table 2 indicating the synthesis of polymer is reproducible. The chemical structures of PBG and PBGA were confirmed by NMR and FTIR (supporting information, Figs. S1 and S2, Table S1). These results of characterization confirmed the successful synthesis of PBG and PBGA.

3.2. Characterization of scaffolds

Photographic images of PBGA scaffold with different MH concentration are shown in Fig. 3. MH is distributed in the scaffolds as indicated by the color change from white to tinted yellow, with the yellow becoming more intense as the concentration of drug increased. The drug MH was incorporated into the polymer in the solution state by mixing them in a mixed solvent of DMAc and THF overnight. The solution compositions are shown in Table S2. Then the solution was used to fabricate fibers via electro spinning process. Thus, the drug is molecularly dispersed in the polymer and its amount will not be affected by the

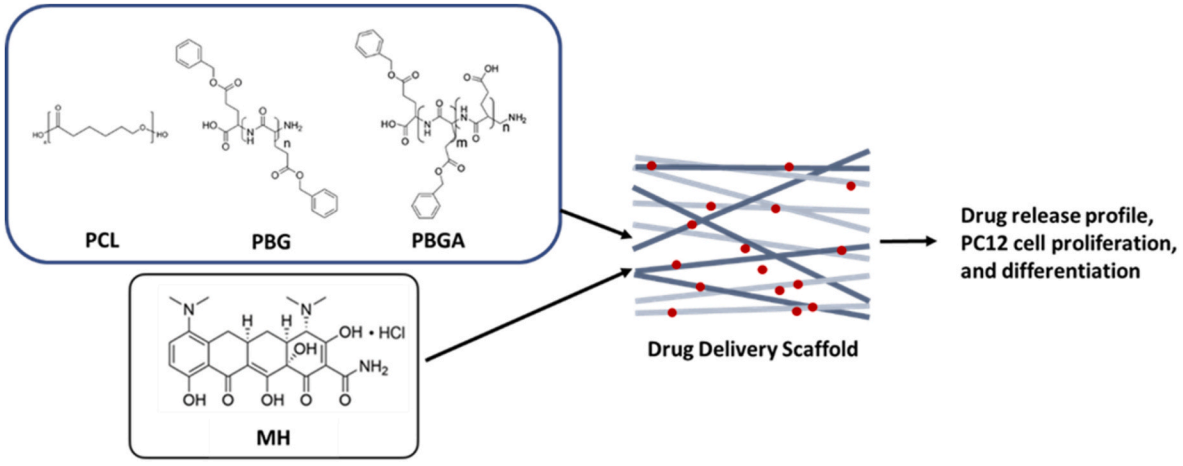

Fig. 1. Schematic diagram of drug delivery system made from electrospun fibrous polymer scaffold and minocycline hydrochloride (MH) for neural tissue engineering.

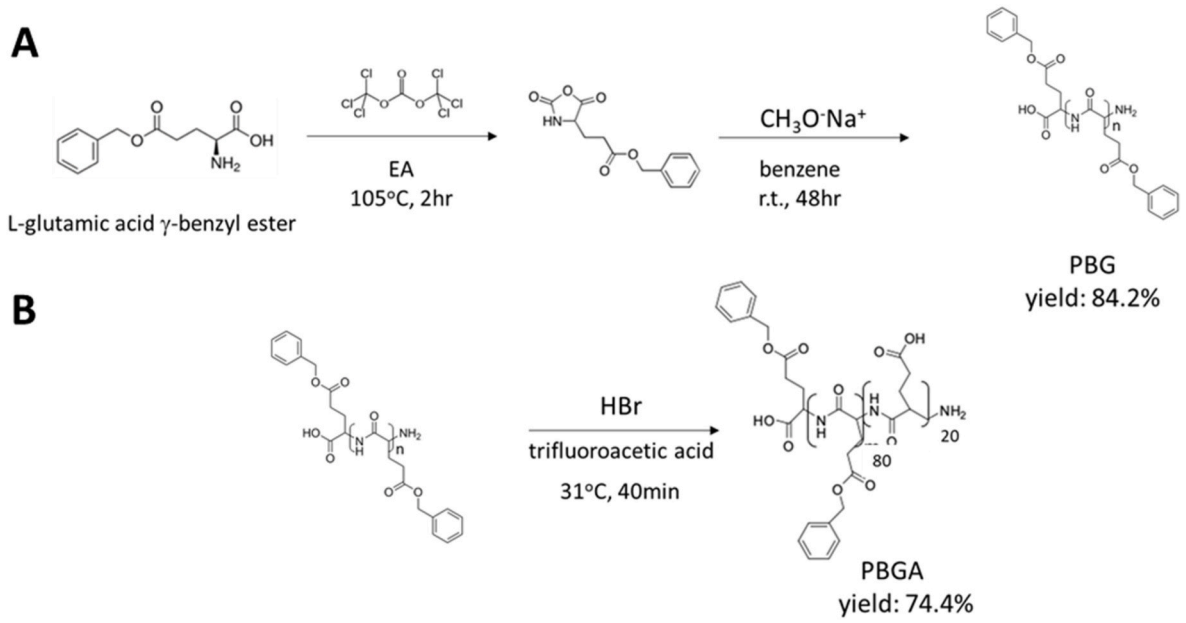

Fig. 2. Synthetic scheme of (A) PBG and (B) PBGA polymers.

Table 2
Properties of polymeric material of PBG including number average molecular weight (Mw), weight average molecular weight (Mw), polydispersity, and yield.

Sample number	Mn (kDa)	Mw (kDa)	Polydispersity	Yield (%)
1	249.2	251.6	1.01	86.7
2	199.9	226.2	1.13	83.5
3	171.2	219.7	1.28	82.4

orientation of fibers. The result indicates the MH can be evenly distributed in the fibers which is important to interpret the drug release mechanism using good reproducible samples. It was been reported the PCL electrospinning fibers can be aligned by rotating collector at rate of more than 1000 rpm [35]. The morphology of electrospun fibers was studied by SEM as shown in Fig. S4 (supporting information). The fibers of polypeptides are straighter and more aligned than those of PCL fibers. We speculate that the polypeptides of PBG and PBGA contain aromatic benzyl group in the repeating unit and hydrogen bonds between peptide linkage of polymer chains make them relatively rigid and easy to align. On the other hand, PCL consists of aliphatic repeating unit of caprolactone and no hydrogen bonds between ester linkage of polymer chains which makes PCL flexible and curvaceous. Thus, PCL is more difficult to align than PBG and PBGA. The results are consistent with the literature report that indicates the Young's modulus of PBG is 4 times higher than that of PCL [36]. The thickness of scaffolds used in the cell culture experiment was in the range of 60 μm with the porosity in the range of 90%. Thus, the scaffolds were indeed in a 3D porous structure to facilitate nutrients flow in the cell culture experiments [29]. The fiber diameter was controlled to be larger than 500 nm for the ease of cell adhesion on the substrate [37] and it was measured by SEM imaging of fibers as shown in Fig. S5. The fiber diameter depends on the polymer type, concentration, conductivity and viscosity of the polymer solution [38]. The effects of MH addition and incorporation upon fiber diameter was investigated. Since MH is a salt, its addition can increase the conductivity of the polymer solution, making the fiber easier to spin and thus reducing fiber diameter. The extend of dimension reduction was decreased by increasing the polarity of the polymer. Therefore, the PBGA polymer exhibited the least amount of reduction in diameter compared to PCL or PBG. It is interesting to observe that the diameter of PCL increased when the concentration MH was increased up to 6 wt%. This might be due to an increase in viscosity, which overcomes the conductivity effect; which subsequently increased the dimension of PCL fibers. The alignment of the fibers in the scaffolds was evaluated and results are discussed in later sections below.

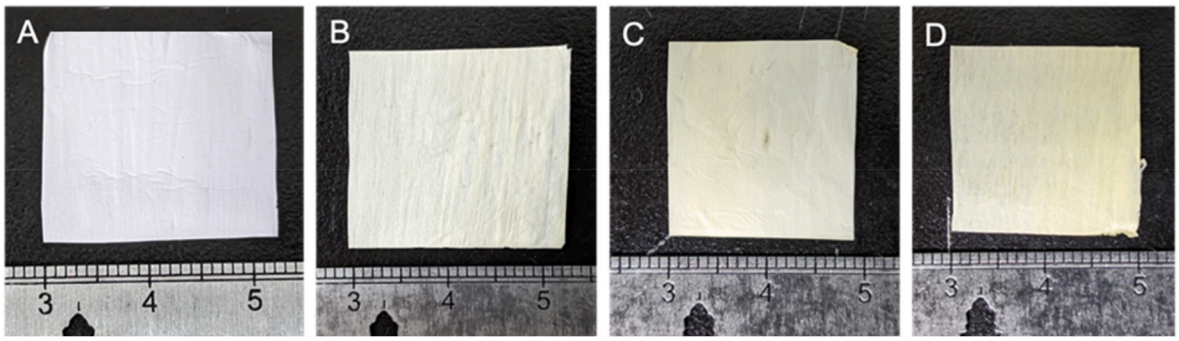

Fig. 3. Photos of (A)PBGA (B)PBGAMH2 (C)PBGAMH4 (D)PBGAMH6 scaffold. The addition of MH can be directly observed by the appearance of yellow color. The yellow becomes intense as the concentration of MH increases. (For interpretation of the references to color in this figure legend, the reader is referred to the Web version of this article.)

3.3. Drug release from scaffolds

During drug release from scaffolds, a cascade of partitioning and diffusion with fibers and dissolution occurs while immersed in PBS. To understand the mechanism behind observed release profiles, known kinetic models of mathematics were used [15,30]. The drug release profile from electrospun fibers is dominated by drug diffusion and material degradation [31,32]. The release profiles from polymer scaffold with various concentrations of MH (2, 4, 6 wt%) within 7 days are shown in Fig. 4. For PCL scaffold, there was a burst of release in the first 24 h, releasing 81.20%, 78.98%, and 80.14% of the drug in 2 wt%, 4 wt%, and 6 wt% MH scaffold, respectively. On the other hand, taking PBGMH4 and PBGAMH4 for instance, the scaffolds only released 22.21% and 28.32% of MH in the first 24 h respectively. The results indicate the drug release from PCL scaffolds are two functions (Fig. 4D black line) due to the burst release of drug initially then follows the logarithm of natural law (Fig. 4A, B, 4C red lines). The drug release of polypeptide scaffolds follows the logarithm of natural law (Fig. 4A, B, 4C blue and green lines), one function equation can be derived (Fig. 4D, E, 4F blue and red lines). The results are very reproducible as indicated in three sets of data of PBG based and PBGA based scaffolds that are compared with PCL scaffolds by varying the loading of the MH drug. The hydrophilicity of the polymers was measured by their water contact angle of dense films as shown in Fig. S6 (supporting information), the average contact angle was 75°, 82°, 76° for PCL, PBG, and PBGA respectively. In the aqueous culture solution, the water-soluble MH is released more readily from the

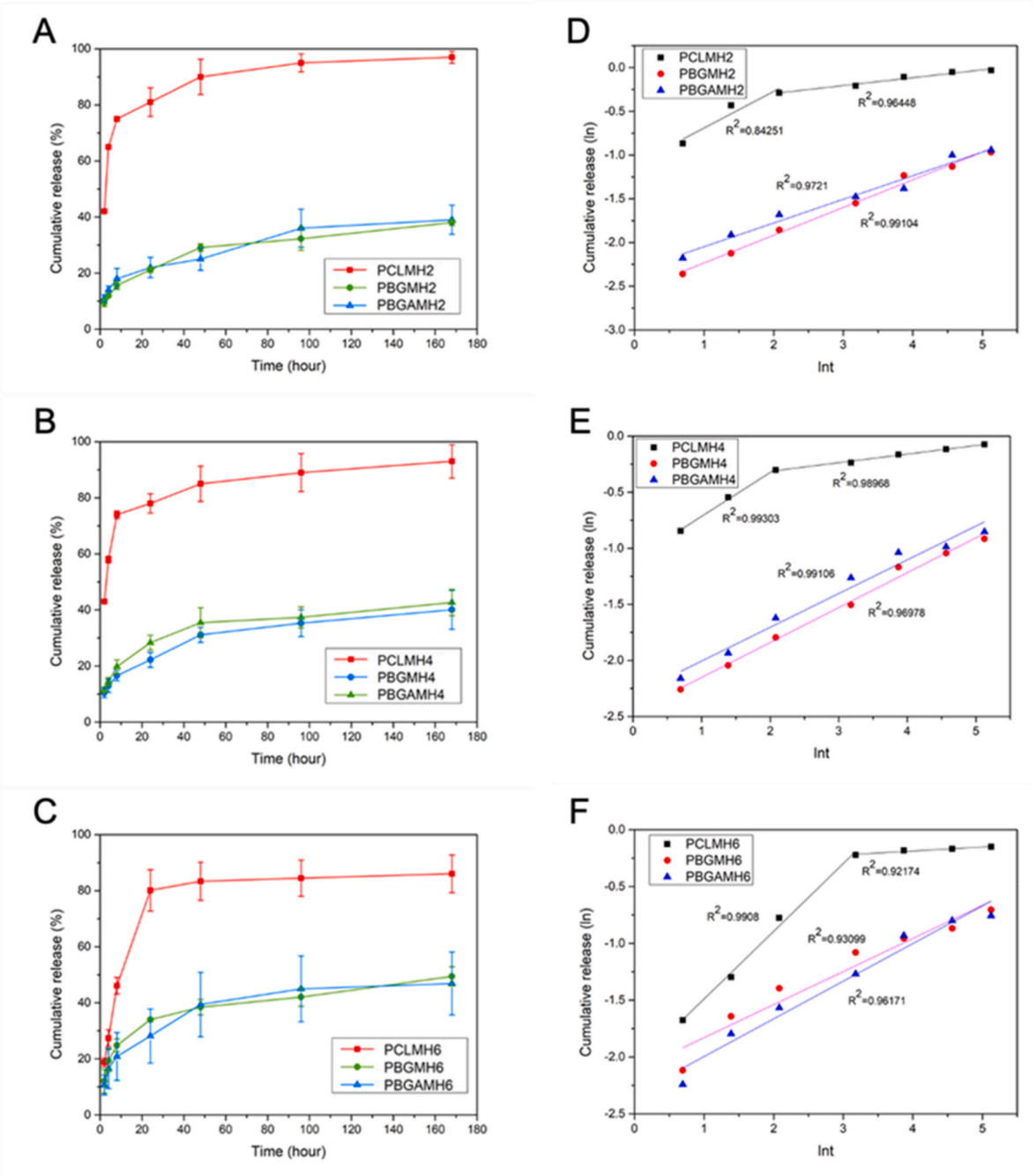

Fig. 4. Minocycline hydrochloride release profile from PCL, PBG, and PBGA scaffolds with three different concentrations in 7 days and the kinetic model fitting results. Release profiles of % cumulative release versus time are shown in (A) (B) (C). Kinetic model fittings are done by plotting nature log value of cumulative release (ln) versus of nature log time (lnt) as shown in (D) (E) (F). Release time points are measured at 2, 4, 8, 24, 48, 96, and 168 h n = 3 for each group.

more hydrophilic polymer, PCL. Although the hydrophilicity of PBGA is close to that of PCL, MH release is slower for PBGA by the increased number of strong hydrogen bonds between PBGA and MH compared to PCL (amide chain versus ester chain).

The release profiles were fitted with two mathematical kinetic models, Higuchi model and Korsmeymer-Peppas model (supporting information, Table S3). The drug release profile can be affected by drug diffusion and carrier degradation [15,33]. The mechanism of drug release kinetics has been explained by several mathematical models, including zero-order equation, first-order equation, Higuchi equation, and Korsmeyer-Peppas equation. Since the drug release profiles show a faster release in the first 24 h and a relatively sustained release thereafter, Korsmeyer-Peppas equation is the most appropriate model to fit the release profile in this study (Fig. 4D, E, F) with $n < 0.45$. The n value of Korsmeyer-Peppas equation can determine the release profile into Fick's diffusion ($n < 0.45$) or non-Fick's diffusion ($0.45 < n < 0.89$) [33]. The former indicates the release profile follows Fick's diffusion, while the latter indicates the release profile is non-Fick's diffuse n, or skeleton degradation. Our previous work demonstrated that the PCL, PBG, and PBGA scaffolds barley degrade in the release duration of 7 days [29]. These results clearly indicate that the MH released from scaffolds examined in this study follow Fick's diffusion law.

3.4. PC12 cell viability on scaffold

The cytotoxicity of each scaffold was evaluated by Live/Dead Assay (Supporting information, Fig. S7). The left figure of Fig. 5 shows that there were more live cells on PBG and PBGA scaffolds than PCL scaffolds after 5-day culturing, denoting that the polypeptide-based scaffolds are less cytotoxic. Moreover, the number of live cells were more numerous on scaffolds with 2 wt% and 4 wt% of MH but, decreased as the drug concentration reached 6 wt%. After 5 days of culturing, the live/dead ratio of cells on PBG scaffolds with 2 wt% and 4 wt% of MH were above 90%, indicating a high degree of biocompatibility.

The right graph of Fig. 5 shows the results of cell viability over day 1, day 3, and day 5 for each scaffold. All the materials containing different MH concentration present increased cell viability index over 5 days of culturing as compared to respective bare scaffold, indicating all the materials are biocompatible. The cell viability was much higher on PBG and PBGA scaffolds than PCL scaffolds and coverslip control group, indicating better adhesion and proliferation on the polypeptide scaffolds. When considering the addition of MH, the cell viability increased linearly for each scaffold. The effect of MH concentration upon viability was best between 0 wt% to 2 wt% and 4 wt%, demonstrating that adding MH promoted cell proliferation. However, when MH concentration increased to 6 wt%, the cell viability index decreases, showing high concentration of MH inhibited the proliferation.

Among all the materials, cells cultured on PBGA scaffold had the highest cell viability. This is likely a result of engineering a polypeptide backbone using the neuron transmitter-like glutamic acid moiety. The PBG scaffold contains benzyl glutamate repeating unit which is different from glutamic acid and is not as effective as the neuron transmitter of glutamic acid [39]. This may explain why PBG shows slightly lower cell viability character than PBGA. Regardless, both the polypeptide PBG and PBGA exhibit better biocompatibility than that of PCL due to their biomimetic structures [29].

To investigate the effect of MH concentration on cellular activity, MH concentration after 24 h *in vitro* was estimated using the fitted release kinetic data above. It is assumed that both release test and cell tests were under similar condition, suggesting the release results can be correlated with the results of cell viability and differentiation. Literature reported that PC12 cells maintain good cell viability and differentiation when the concentration of MH was at 30 μM [24]. We found PC12 viability increased incrementally with MH concentration up to 4 wt% but decreased in cell viability at 6 wt%. After 24 h *in vitro* experiments, the scaffold contained 4 wt% MH is estimated from the kinetic model to be 38.3 μM for PBGMH4, 49.5 μM for PBGAMH4. For the scaffold contained 6 wt% MH, the estimated value is 94.8 μM for PBGMH6 and 78.6 μM for PBGAMH6 (supporting information, Table S4). Thus, we speculate that the high concentration of MH may induce cytotoxicity thus lower the cell viability. To sum up, both Alamar blue test and live and death assay performance show the PBGA scaffold with 4 wt% MH exhibited the highest cell viability.

3.5. PC12 cell differentiation and neurite growth on scaffold

Cell differentiation and neurite outgrowth were investigated by SEM (Fig. 6) and cytoskeletal staining of PC12 cells (supporting information, Fig. S8). PC12 was stimulated by exogenous NGF for five days and neurite elongation was assessed. To quantify the results of neurite formation and extension, neurite lengths were measured by software ImageJ and statistically analyzed (Fig. 7). The results of cell differentiation are similar as those of cell toxicity and cell viability. The effects of material type of scaffolds on cell differentiation demonstrate that PC12 have longer neurites on PBG and PBGA scaffolds than PCL scaffolds. The neurite lengths increased with MH increment up to 4 wt% but decreased when the MH concentration exceeded 4 wt%. The neurite lengths of PC12 cells were significantly longer on PBGA scaffold with 4 wt% of MH

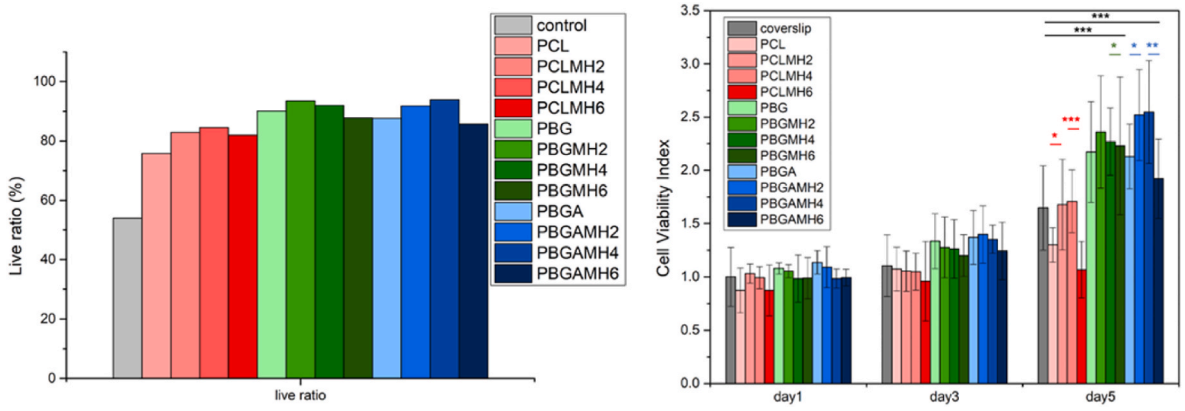

Fig. 5. Biocompatibility of PC12 cells on polymer scaffold after 5-day culture in terms of mean average ratio of live cells to dead cells (left) and cell viability index (right). PBG series scaffolds show higher live/dead ratio than control group (coverslip) and PCL series scaffolds, indicating better biocompatibility. Each group was repeated three times. 5–6 pictures were taken at different spot for each group, then the average value was used to make the plot as shown in the left of Fig. 3. The cell viability was determined by normalizing the percentage of cell reduction on each scaffold to the coverslip as control at day 1. Each group was repeated for 3 times. H test: *** indicates $p \leq 0.001$, ** indicates $p \leq 0.01$, and * indicates $p \leq 0.05$.

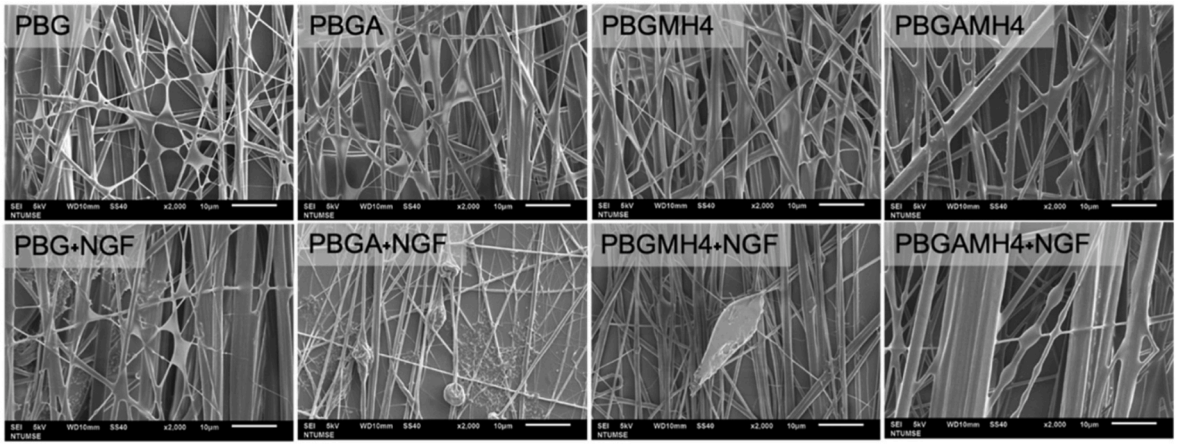

Fig. 6. SEM images of PC12 cell growth and cell differentiation (with 100 ng/mL NGF) for five days on PBG, PBGA, PBGMH4, and PBGAMH4 scaffold. PC12 cells demonstrate good adhesion on the scaffolds. With the addition of NGF, the neurite outgrowth extends along the direction of the fibers. Scale bar = 10 μm.

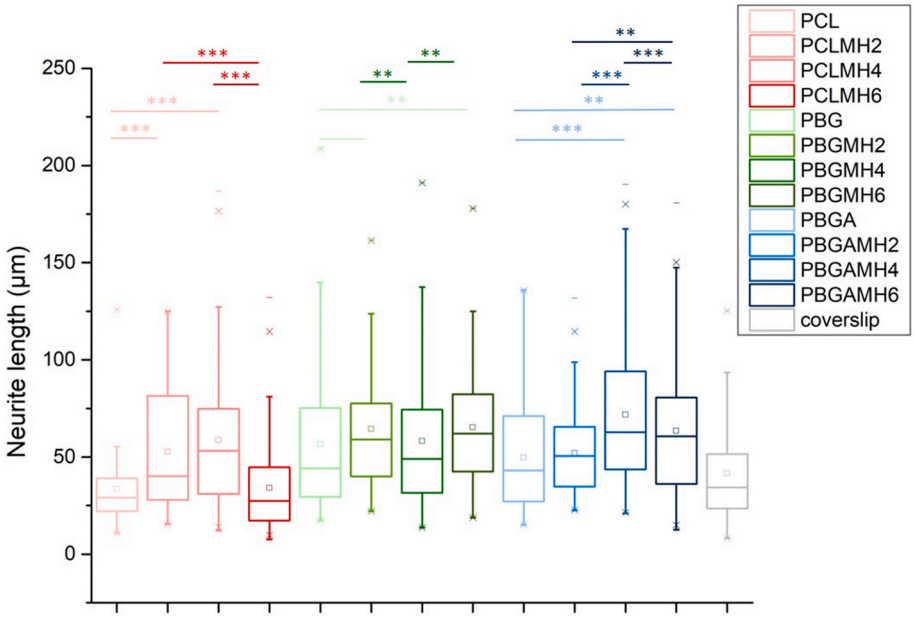

Fig. 7. Box chart of PC12 neurite lengths after 5-day differentiation. Each group was repeated for 3 times. 10–20 fluorescence pictures were taken from different area of each group. Neurite counts = 77–126 in each group. H test: *** indicates $p \leq 0.001$, ** indicates $p \leq 0.01$, and * indicates $p \leq 0.05$.

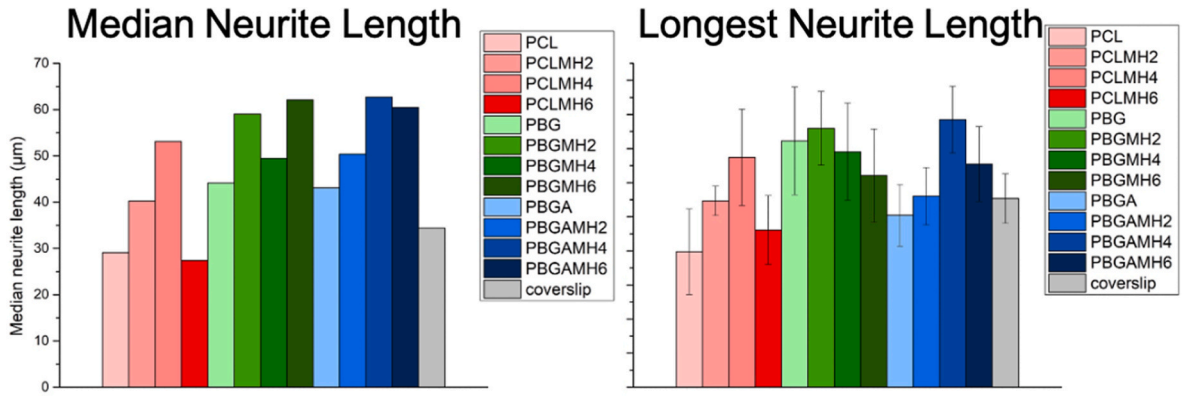

Fig. 8. Diagrams of the average median neurite length and longest neurite length of PC12 cells after 5-day differentiation. Each group was repeated for 3 times.10–20 fluorescence pictures were taken from different area of each group. Neurite counts = 77–126 in each group. The only one neurite length ranking in the middle was selected as the median neurite length (left figure). The longest 10% of neurites of each group were selected and averaged as the longest neurite length (right figure).

than other groups. Moreover, if comparing median and longest neurite length among different scaffolds with various MH concentration, the same conclusions is found. That is the cell culture on PBGA4MH produced longest and highest median neurite length (Fig. 8). The trend of neurite length follows the results of cell viability.

Misdirected axonal regeneration and the failure of long range axonal regeneration challenge the restoration of disrupted nervous systems. The neurite outgrowth orientation was analyzed and plotted by polar chart (supporting information, Fig. S9). The neurites are more aligned on PBG and PBGA scaffolds with various concentration of MH than PCL scaffolds and the control group coverslips. This directionality most likely results from an increased guidance by aligned fibers in polypeptide scaffolds (Fig. S10). Indeed, others have reported the effects of alignment and contact inhibition of neurite extension [34,40]. Increased alignment of neurites extending on PBG and PBGA suggests that neurites can extend along the polypeptide scaffolds successfully, and the addition of MH does not affect the direction of neurite on the fibers.

3.6. Comparing the orientation of neurite extension with the orientation fibers in scaffold

Normal neurophysiology requires developing neurons to target and form appropriate synapses with target cells, often over great distances (such as from retinal ganglion cells to the brain cortex). Neurons communicate using neurotransmitter that are synthesized and then transported from soma to the axon tip. As such, restoration of compromised nervous systems and accompanying cytoarchitecture can be enhanced by the engineering the alignment of neurite outgrowth. This alignment and directionality can be controlled by the orientation of fibers in the scaffold. Others have shown that in the context of the peripheral nervous system, aligned fibrous graphene based scaffold produce the anisotropic structure of the native sciatic nerve [41]. The degree of orientation of fibers in our scaffolds was determined by software ImageJ using polar chart derived from SEM photos of scaffolds shown in Fig. S4. The results are shown in Fig. S10. The degree of orientation of fibers and neurites in scaffold are defined as the percentage of fibers or neurites aligned in the degree of $0 \pm 15^{\circ}$ and $180 \pm 15^{\circ}$ of the images. The results are summarized in Table 3. The degree of orientation of fibers in each scaffold was all above 50%, indicating that fibers were well aligned. The result of neurite orientation also demonstrates that the outgrowth of neurite extends in specific direction, especially for PBG scaffold and PBGA scaffold, demonstrating that the polypeptide scaffolds with aligned fibers could successfully guide the outgrowth of neurites.

Table 3
Degree of orientation of fibers and neurite outgrowth on different scaffolds.

Material	% Orientation of fibers[a]	% Orientation of neurites[b,c]
PCL	76.92	49.41
PCLMH2	67.92	29.05
PCLMH4	66.67	30.84
PCLMH6	57.14	36.94
PBG	63.64	67.74
PBGMH2	73.68	80.02
PBGMH4	60.87	80.52
PBGMH6	72.50	79.52
PBGA	72.22	51.56
PBGAMH2	82.35	64.82
PBGAMH4	71.05	71.73
PBGAMH6	63.13	77.12

[a] **Degree of orientation of fibers** is defined by the percentage of fibers oriented in the range of $0 \pm 15^{\circ}$ and $180 \pm 15^{\circ}$ of the polar images of fibers. Showing the fibers of scaffolds are aligned well.
[b] **Degree of orientation of neurite outgrowth on different scaffold**. Showing the neurites grown along the orientation of fibers in scaffolds.
[c] Degree of orientation of neurite outgrowth on coverslip is 24.99%.

4. Conclusions

We have established a drug delivery system composed of polypeptide-based electrospun fibers and the neuroprotective antibiotic MH for neural tissue engineering. Two polypeptides PBG and PBGA were studied, which contain neuronal stimulant glutamate and glutamic acid, and PCL was used as a comparative control. The release profiles of MH from the scaffolds were systematically studied. Due to the strong hydrogen bonding of PBGA scaffold and hydrophobicity of PBG scaffold, MH showed sustained release from these novel scaffolds with significant improvement over the transient release from PCL scaffold. The release profiles follow Fick's diffusion law. Cell viability and differentiation on the scaffolds were investigated using neuronal PC12 in *in vitro* experiments. Comparing different materials with various MH concentrations, PBGA scaffold with 4 wt% MH demonstrates the highest cell viability, suggesting that neurotransmitter-like functional group and adequate MH concentration enhances biocompatibility. Cell viability and the neurite length were seen to decrease as MH concentration increases to 6 wt% although this cytotoxicity could differ in animal rather than cell culture models. After five days of cell differentiation, the neurite outgrowth was best on the PBGA scaffold with 4 wt% MH. The neurite length median of this scaffold reaches 62.71 μm, and the maximum length was 190.29 μm. This represents a four-fold increase over median neurite length produced on pristine PBGA scaffold (47.07 μm). Altogether, the results indicate that the PBGA scaffold with 4 wt% of MH (PBGAMH4) represents a promising drug delivery system without external stimulations in cell culture for neural tissue engineering. This novel biocompatible and bio-functional scaffold is quite simple in chemical composition which has never been reported in the literature. The scaffolds are fabricated from polypeptide which contains built in drug MH and nerve stimulating moiety of glutamate. They have potential applications in neural tissue engineering to repair and regeneration of central nervous system or peripheral nervous system.

CRediT authorship contribution statement

An-Jey A. Su: Writing – original draft, preparation, Methodology. **Ning Jiang:** Validation, Investigation. **Shyh-Chyang Luo:** Resources. **Kia M. Washington:** Resources, Methodology. **Ming-Chung Wu:** Resources, Visualization. **Yu-Ching Huang:** Visualization, Writing – review & editing, Project administration, Funding acquisition. **Wei-Fang Su:** Conceptualization, Supervision, Writing – review & editingWriting-Reviewing and Editing.

Declaration of competing interest

The authors declare that they have no known competing financial interests or personal relationships that could have appeared to influence the work reported in this paper.

Data availability

No data was used for the research described in the article.

Acknowledgment

We thank the financial supports for this research from Ministry of Science and Technology of Taiwan (MOST 108-2221-E-002-027-MY3, MOST 110-2221-E-131-010, MOST 111-2221-E-131-022, MOST 111-2221-E-002-029), Department of Defense of USA (W81XWH-16-1-0775) and University of Colorado Anschutz Medical Campus, USA (Su AEF Seed Grant: 63503960).

Appendix A. Supplementary data

Supplementary data to this article can be found online at https://doi.

org/10.1016/j.matchemphys.2023.127974.

References

[1] L. Bertram, R.E. Tanzi, The genetic epidemiology of neurodegenerative disease, J. Clin. Investig. 115 (2005) 1449–1457.
[2] A. Kumar, A. Singh, A review on Alzheimer's disease pathophysiology and its management: an update, Pharmacol. Rep. 67 (2015) 195–203.
[3] F.G. Jennekens, A short history of the notion of neurodegenerative disease, J. Hist. Neurosci. 23 (2014) 85–94.
[4] M. Curcio, F. Bradke, Axon regeneration in the central nervous system: facing the challenges from the inside, Annu. Rev. Cell Dev. Biol. 34 (2018) 495–521.
[5] A. Benga, F. Zor, A. Korkmaz, B. Marinescu, V. Gorantla, The neurochemistry of peripheral nerve regeneration, Indian J. Plast. Surg. 50 (2017) 5–15.
[6] C.E. Schmidt, J.B. Leach, Neural tissue engineering: strategies for repair and regeneration, Annu. Rev. Biomed. Eng. 5 (2003) 293–347.
[7] I.P. Clements, J.M. Munson, R.V. Bellamkonda, in: B.D. Ratner, A.S. Hoffman, F. J. Schoen, J.E. Lemons (Eds.), Neuronal Tissue Engineering in, Biomaterials Science, Elsevier, 2013, pp. 1291–1306.
[8] G.D. Mogoşanu, A.M. Grumezescu, L. Mogoantă, L.E. Bejenaru, C. Bejenaru, Applications of nanobiopolymers for soft tissue engineering, in: A.M. Grumezescu (Ed.), Nanobiomaterials in Soft Tissue Engineering, Elsevier, 2016, pp. 83–109.
[9] M.E. Gomes, M.T. Rodrigues, R.M. Domingues, R.L. Reis, Tissue engineering and regenerative medicine: new trends and directions—a year in review, Tissue Eng. B Rev. 23 (2017) 211–224.
[10] R. Boni, A. Ali, A. Shavandi, A.N. Clarkson, Current and novel polymeric biomaterials for neural tissue engineering, J. Biomed. Sci. 25 (2018) 1–21.
[11] R.K. Willits, S.L. Skornia, Effect of collagen gel stiffness on neurite extension, J. Biomater. Sci. Polym. Ed. 15 (2004) 1521–1531.
[12] L.L. Norman, H. Aranda-Espinoza, Cortical neuron outgrowth is insensitive to substrate stiffness, Cell. Mol. Bioeng. 3 (2010) 398–414.
[13] J. Doshi, D.H. Reneker, Electrospinning process and applications of electrospun fibers, J. Electrost. 35 (1995) 151–160.
[14] F. Yang, R. Murugan, S. Wang, S. Ramakrishna, Electrospinning of nano/micro scale poly (L-lactic acid) aligned fibers and their potential in neural tissue engineering, Biomaterials 26 (2005) 2603–2610.
[15] Y. Ding, W. Li, F. Zhang, Z. Liu, N. Zanjanizadeh Ezazi, D. Liu, H.A. Santos, Electrospun fibrous architectures for drug delivery, tissue engineering and cancer therapy, Adv. Funct. Mater. 29 (2019), 1802852.
[16] M.T. Lin, M.F. Beal, Mitochondrial dysfunction and oxidative stress in neurodegenerative diseases, Nature 443 (2006) 787–795.
[17] S.E. Seidl, J.A. Potashkin, The promise of neuroprotective agents in Parkinson's disease, Front. Neurol. 2 (2011) 68.
[18] M. Domercq, C. Matute, Neuroprotection by tetracyclines, Trends Pharmacol. Sci. 25 (2004) 609–612.
[19] Z. Xia, R.M. Friedlander, Minocycline in multiple sclerosis — compelling results but too early to tell, N. Engl. J. Med. 376 (2017) 2191–2193.
[20] H.-S. Kim, Y.-H. Suh, Minocycline and neurodegenerative diseases, Behav. Brain Res. 196 (2009) 168–179.
[21] M. Chen, V.O. Ona, M. Li, R.J. Ferrante, K.B. Fink, S. Zhu, J. Bian, L. Guo, L. A. Farrell, S.M. Hersch, Minocycline inhibits caspase-1 and caspase-3 expression and delays mortality in a transgenic mouse model of Huntington disease, Nat. Med. 6 (2000) 797–801.
[22] X. Wang, S. Zhu, M. Drozda, W. Zhang, I.G. Stavrovskaya, E. Cattaneo, R. J. Ferrante, B.S. Kristal, R.M. Friedlander, Minocycline inhibits caspase-independent and-dependent mitochondrial cell death pathways in models of Huntington's disease, Proc. Natl. Acad. Sci. USA 100 (2003) 10483–10487.
[23] C.J. Garwood, J.D. Cooper, D.P. Hanger, W. Noble, Anti-inflammatory impact of minocycline in a mouse model of tauopathy, Front. Psychiatr. 1 (2010) 136.
[24] K. Hashimoto, T. Ishima, A novel target of action of minocycline in NGF-induced neurite outgrowth in PC12 cells: translation initiation factor eIF4AI, PLoS One 5 (2010), e15430.
[25] C. Li, K. Yuan, H. Schluesener, Impact of minocycline on neurodegenerative diseases in rodents: a meta-analysis, Rev. Neurosci. 24 (2013) 553–562.
[26] M.L. Garcez, F. Mina, T. Bellettini-Santos, A.P. da Luz, G.L. Schiavo, J.M. C. Macieski, E.B. Medeiros, A.O. Marques, N.Q. Magnus, J. Budni, The involvement of NLRP3 on the effects of minocycline in an AD-like pathology induced by β-amyloid oligomers administered to mice, Mol. Neurobiol. 56 (2019) 2606–2617.
[27] J. Zhou, K.R. Ledesma, K.-T. Chang, H. Abodakpi, S. Gao, V.H. Tam, Pharmacokinetics and pharmacodynamics of minocycline against Acinetobacter baumannii in a neutropenic murine pneumonia model, Antimicrob. Agents Chemother. 61 (2017), e02371-16.
[28] B. Wang, Y. Wang, T. Yin, Q. Yu, Applications of electrospinning technique in drug delivery, Chem. Eng. Commun. 197 (2010) 1315–1338.
[29] Z.H. Wang, Y.Y. Chang, J.G. Wu, C.Y. Lin, H.L. An, S.C. Luo, T.K. Tang, W.F. Su, Novel 3D neuron regeneration scaffolds based on synthetic polypeptide containing neuron cue, Macromol. Biosci. 18 (2018) 1700251–1700263.
[30] R. Gouda, H. Baishya, Z. Qing, Application of mathematical models in drug release kinetics of carbidopa and levodopa ER tablets, J. Dev. Drugs 6 (2017) 1–8.
[31] X. Li, M.A. Kanjwal, L. Lin, I.S. Chronakis, Electrospun polyvinyl-alcohol nanofibers as oral fast-dissolving delivery system of caffeine and riboflavin, Colloids Surf., B 103 (2013) 182–188.
[32] U. Angkawinitwong, S. Awwad, P.T. Khaw, S. Brocchini, G.R. Williams, Electrospun formulations of bevacizumab for sustained release in the eye, Acta Biomater. 64 (2017) 126–136.
[33] J. Wu, Z. Zhang, W. Zhou, X. Liang, G. Zhou, C.C. Han, S. Xu, Y. Liu, Mechanism of a long-term controlled drug release system based on simple blended electrospun fibers, J. Contr. Release 320 (2020) 337–346.
[34] P. Wang, Y. Sun, X. Shi, H. Shen, H. Ning, H. Liu, Bioscaffolds embedded with regulatory modules for cell growth and tissue formation: a review, Bioact. Mater. 6 (2021) 1283–1307.
[35] S.N. Gorodzha, M.A. Surmeneva, R.A. Surmenev, Fabrication and characterization of polycaprolactone cross- linked and highly-aligned 3-D artificial scaffolds for bone tissue regeneration via electrospinning technology, IOP Conf. Ser. Mater. Sci. Eng. 98 (2015), 012024.
[36] T.-L. Ma, S.-C. Yang, T. Cheng, M.-Y. Chen, J.-H. Wu, S.-L. Liao, W.-L. Chen, W.-F. Su, Exploration of biomimetic poly(γ-benzyl-l-glutamate) fibrous scaffolds for corneal nerve regeneration, J. Mater. Chem. B 10 (2022) 6372–6379.
[37] P.-H. Chen, H.-C. Liao, S.-H. Hsu, R.-S. Chen, M.-C. Wu, Y.-F. Yang, C.-C. Wu, M.-H. Chen, W.-F. Su, A novel polyurethane/cellulose fibrous scaffold for cardiac tissue engineering, RSC Adv. 5 (2015) 6932–6939.
[38] F. Yalcinkaya, B. Yalcinkaya, O. Jirsak, Influence of salts on electrospinning of aqueous and nonaqueous polymer solutions, J. Nanomater. 2015 (2015), 134251.
[39] C.-Y. Lin, S.-C. Luo, J.-S. Yu, T.-C. Chen, W.-F. Su, Peptide-based polyelectrolyte promotes directional and long neurite outgrowth, ACS Appl. Bio Mater. 2 (2018) 518–526.
[40] I. Tonazzini, C. Masciullo, E. Savi, A. Sonato, F. Romanato, M. Cecchini, Neuronal contact guidance and YAP signaling on ultra-small nanogratings, Sci. Rep. 10 (2020) 1–18.
[41] N. Golafshan, M. Kharaziha, M. Fathi, B.L. Larson, G. Giatsidis, N. Masoumi, Anisotropic architecture and electrical stimulation enhance neuron cell behaviour on a tough graphene embedded PVA: alginate fibrous scaffold, RSC Adv. 8 (2018) 6381–6389.